Photoelectrode/Electrolyte interfacial band lineup engineering with alloyed III-V thin films grown on Si substrate.

Mekan Piriyev, Gabriel Loget, Yoan Léger, Vi Hanh Le, Lipin Chen, Antoine Létoublon, Tony Rohel, Christophe Levallois, Julie Le Pouliquen, Bruno Fabre, et al.

ARTICLE

Photoelectrode/Electrolyte interfacial band lineup engineering with alloyed III-V thin films grown on Si substrate.

Received 00th January 20xx,
Accepted 00th January 20xx

DOI: 10.1039/x0xx00000x

Mekan Piriyev[a], Gabriel Loget[b], Yoan Léger[a], Hanh Vi Le[c], Lipin Chen[a, c],Antoine Létoublon[a], Tony Rohel[a], Christophe Levallois[a], Julie Le Pouliquen[a], Bruno Fabre[b], Nicolas Bertru[a,*], Charles Cornet[a,*]

In this work, we demonstrate how the classical concept of band gap engineering usually used in III-V semiconductor devices can be extended to the engineering of the band lineup between semiconducting photoelectrodes and electrolytes. The performance of photoelectrodes made of $GaP_{1-x}As_x$ epilayers in the full compositional range and grown on low-cost Si substrates were studied and compared with photoelectrodes elaborated on GaAs and GaP substrates. We first show that the changes of the Incident Photon to Current conversion Efficiency (IPCE) with the As content in $GaP_{1-x}As_x$ alloys are related to the band gap nature (direct or indirect) and band gap energy variations. Then, from flat band potential measurements during Mott-Schottky experiments, valence and conduction band energies of $GaP_{1-x}As_x$ alloys are positioned versus reversible hydrogen potential. A weak change of conduction band energies and a large evolution of the valence band energies are obtained, in good agreement with expected theoretical trends. Such results show that both band gap and semiconductor/electrolyte band lineups can be engineered through alloying of III-V semiconductors deposited on silicon substrates. This band lineup engineering strategy is expected to be of great interest to address specific redox reactions in the electrolyte, provided that suitable protecting or passivating layers can be used to limit surface/interface recombinations.

A 1. Introduction

The production of hydrogen directly from the solar energy is considered as one of the promising pathways to store renewable energy.[1,2] Photo-Electro-Chemical (PEC) cells have emerged as potential candidates for converting and storing solar energy into hydrogen, similarly to natural photosynthesis.[3,4] However, renewable production of H_2 in PEC cells remains today costly, due to the low efficiency, and/or the high fabrication cost of production systems.[1,5] Semiconductor (SC) photoelectrodes are at the core of PEC systems. The choice of the SC is therefore crucial to achieve both high solar-to-hydrogen (STH) efficiency and low production cost.[6,7] The ideal semiconducting material must combine,[8] (i) a direct band gap, not too large, in order to ensure large solar light absorption, (ii) appropriate energy band positions versus water splitting half-reactions to reduce electrode overpotentials, and (iii) a cost-effective fabrication, to reduce the levelized cost of hydrogen production. Huge research efforts have been devoted to find new materials or material associations that possess all these characteristics.[1,6]

Because of their remarkable optical and transport properties, III-V semiconductors have been extensively used in solar cells, sensors and photonics devices, both at academic and at industrial levels.[9,10] Most of these achievements were not made with binary compounds but with stacks of III-V alloys which allow to tune band gaps and band lineups. This strategy, often referred to as "band gap engineering"[11] consists in alloying different binary III-V semiconductors to form alloys, with targeted band gap properties for laser emission or light harvesting.[12] Over the years, different epitaxial setups such as Molecular Beam Epitaxy (MBE) or Metal-Organic Chemical Vapor Deposition (MOCVD) have been developed. They

[a] Univ Rennes, INSA Rennes, CNRS, Institut FOTON – UMR 6082, F-35000Rennes, France.
[b] Univ Rennes, CNRS, ISCR (Institut des Sciences Chimiques de Rennes)–UMR6226, F-35000 Rennes, France
[c] Tianjin Key Laboratory of Film, Electronic and Communication Devices, School of Integrated Circuit Science and Engineering, Tianjin University of Technology, Tianjin 300384, China

* Corresponding authors, Charles.cornet@insa-rennes.fr; Nicolas.bertru@insa-rennes.fr;

Electronic Supplementary Information (ESI) available: [details of any supplementary information available should be included here]. See DOI: 10.1039/x0xx00000x

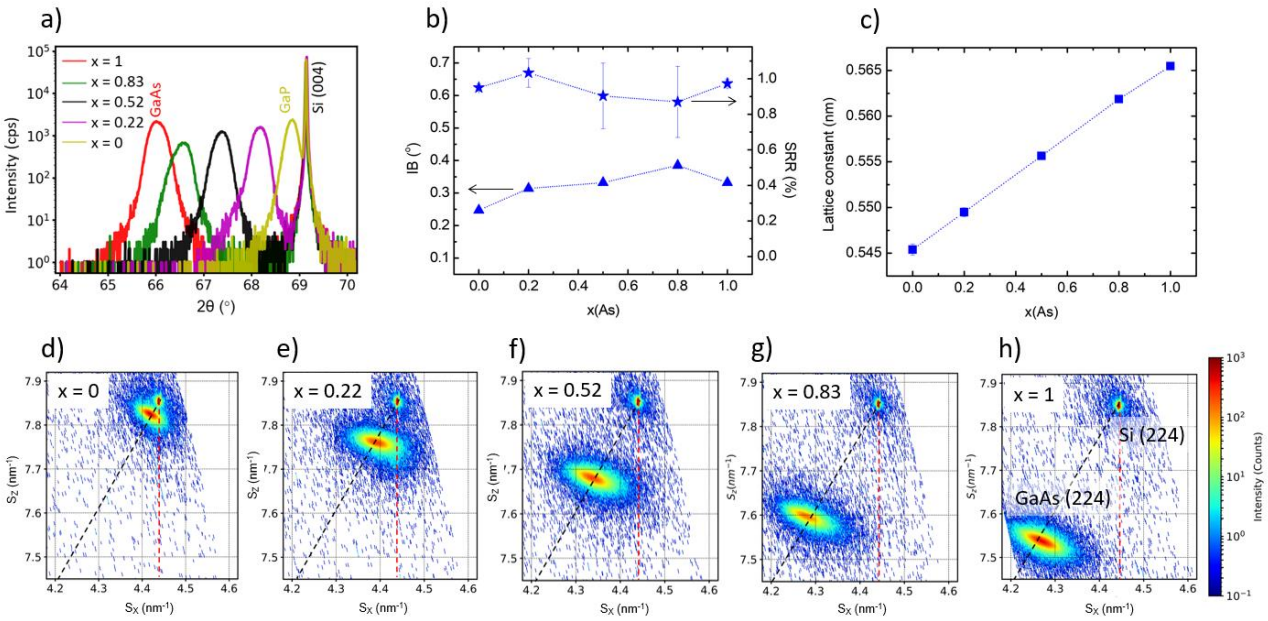

Fig. 1 (a) X-Ray Diffraction ω/2θ scans performed in the vicinity of Si (004) for the different $GaP_{1-x}As_x$ /Si samples; (b) Evolution of the integral breadth (IB) of the epilayer Bragg peak (triangle) and strain relaxation rate (SRR) (star) as a function of x(As); (c) Evolution of the measured lattice constant vs x(As); (d-h) Reciprocal Space Maps showing the Si substrate and the epilayer (224) Bragg peaks with the black dashed line representing the fully plastically relaxed line and the red dashed line representing the fully elastically strained line for the different samples (the x(As) content is given in the inset).

routinely allow the elaboration of III-V alloys with composition fluctuations lower than 1% over a 4-inch wafer. III-V semiconductors were considered also in PEC cells, but the vast majority of the reports focus on binary compounds for which PEC cells with relatively high photocurrents and photovoltages were demonstrated.[13-17] However, band gaps and semiconductor band edge energies with respect to redox levels are fully determined by binary III-V properties and cannot be optimized. Only few photoelectrodes using ternary III-V alloys were achieved yet. As an example, a (GaInP/GaInAs)/TiO_2/RuO_x multiple-junction photoelectrode has been used to operate unassisted water splitting with 19% of STH efficiency.[18] In these devices,[6,19] alloying is mostly used to adjust the band gaps of the multiple absorbers to the sunlight spectrum and to ensure current matching between p-n junctions. The optimization of the SC band edge alignments with water redox levels was not considered.

A major drawback of III-V based PEC cells are their prohibitively high cost. The main part originates from substrates, which represents 90% of the final device cost.[20] Recently, photoelectrodes based on III-V thin films directly grown on low cost Si substrates were proposed, leading to a drastic cost reduction.[21-24] Following this strategy, band gap engineering was proposed theoretically to address the issue of band alignments between the semiconducting photoelectrodes and redox levels of the electrolyte, but without a clear experimental proof of the concept in electrochemistry.[25]

In this work, we assess experimentally the opportunities offered by III-V alloys to tune at will the band lineups between semiconductor band energies and electrolyte water redox levels. For this purpose, we study the photoelectrochemical performance of photoelectrodes, made from $GaP_{1-x}As_x$ alloys epitaxially grown on a cost-effective Si substrate. We show how both optical and photoelectrochemical properties can be adjusted through the fine control of the As composition in the alloys. By varying the composition, the absorption edge is tuned from 1.39 to 2.41 eV. The nature of the band structure (indirect or direct) is also modified as deduced from the change of photon-to-current conversion efficiency. The variation of flat-band potentials (V_{fb}) as a function of the As content is determined from Mott-Schottky (MS) measurements. From this analysis, and the subsequent conduction and valence band positioning versus the RHE, we show that the band lineup between the photoelectrode and the electrolyte can be engineered by using alloying. Finally, we discuss the influence of surface recombination and low hole transfer kinetics on the performance of these bare photoelectrodes without passivation or catalyst layers.

B. Experimental section

Materials. 1 μm-thick $GaP_{1-x}As_x$ alloys with targeted compositions being x = 0 (GaP), 0.2, 0.5, 0.8 and 1 (GaAs) were grown by Molecular Beam Epitaxy (MBE) on a n-doped Si substrate (Sil'tronix Silicon Technologies). The $GaP_{1-x}As_x$ layers were non intentionally doped. Commercial n-doped GaAs (referred as GaAs:n) and GaP (referred as GaP:n) wafers (Wafer Technology Ltd.) with thicknesses of 350 µm were used as the reference samples to compare photoelectrochemical properties. (Details are given in **Table S1** in Supplementary Data)

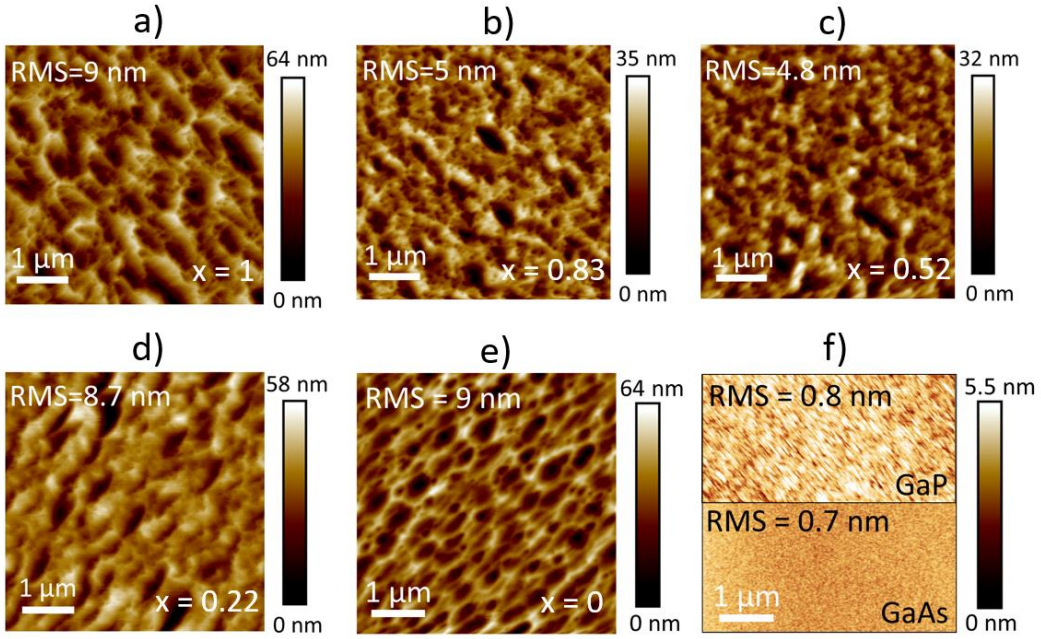

Fig. 2 Surface topography obtained from atomic force microscopy (a-e) for the epitaxial $GaP_{1-x}As_x$ alloys on Si with different x(As) and (f) for the commercial GaP and GaAs wafers

Photoanode preparation. Prior to the preparation of the Photoanodes (PAs), all the epitaxial samples composed of $GaP_{1-x}As_x$ alloys on Si were cleaned in ultrasound cleaner for 10s with ultrapure water and subsequently purged with a flow of N_2 gas. The backside was scratched to make ohmic contact using Gallium-Indium eutectic (99.99%, Alfa Aesar) and silver paste (Electron Microscopy Sciences). The electrochemically active surface area was defined using an epoxy resin (EA 3423, Henkel from Loctite) covering backside and edges of the PA and was measured with ImageJ software. The detailed description of the characterization methods and corresponding additional figures are given in Supplementary Data.

C. Results and discussion

The structural characterization of the epitaxial $GaP_{1-x}As_x$ /Si alloys was first carried out using X-Ray Diffraction (XRD) in conventional ω/2θ mode. **Figure 1a** shows a superimposed plot of ω/2θ scans performed in the vicinity of Si (004) for the different samples. The ω/2θ scans exhibit a common thin Bragg peak at 69.13°, which is related to the Si substrate. The other well-defined Bragg peaks are related to $GaP_{1-x}As_x$ layers. Their Integral Breadths (IB) (**Figure 1b,** triangle markers) are similar, indicating a comparable crystal quality, independently of the alloy composition. The positions of the $GaP_{1-x}As_x$ Bragg peaks depend on alloy compositions and on strain status of the epilayers. In order to separate both effects and to determine accurately $GaP_{1-x}As_x$ alloys composition, Reciprocal Space Maps (RSM) were recorded around (224), (**Figure 1 (d-h)**), (-224) and (004) (**Figure S1**) diffraction peaks. The Strain Relaxation Rates (SRR) were then inferred for each layer. A SRR = 1 corresponds to a fully plastically relaxed layer, while a SRR = 0 corresponds to a fully elastically strained layer. On all $GaP_{1-x}As_x$ /Si samples,

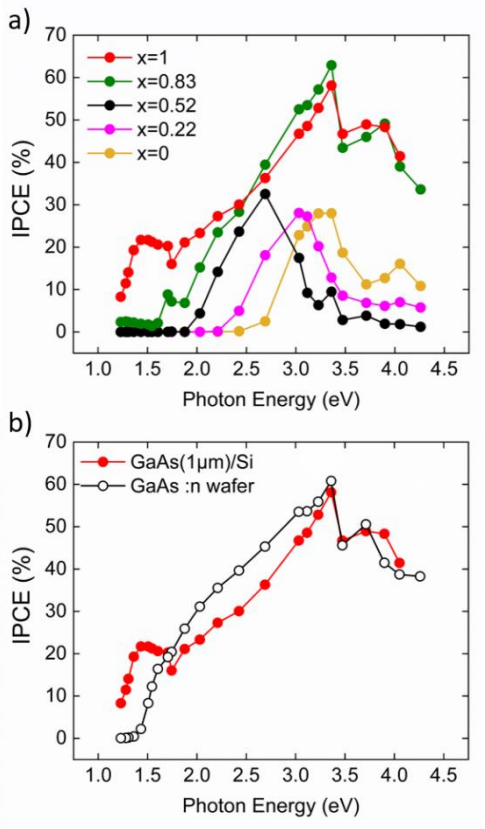

Fig. 3 (a) IPCE spectra for the 1 µm-thick epitaxial $GaP_{1-x}As_x$ alloys grown on Si substrate measured under polychromatic light (1 sun) at 1 V vs RHE applied potential; (b) Comparison of the IPCE spectra of the GaAs (1 µm)/Si epilayer and bare n-doped GaAs:n wafer (350 µm-thick) measured in the same conditions

a SRR larger than 0.85, is determined from RSM (**Figure 1b** – star markers) indicating that the epitaxial layers are close to the perfect plastic relaxation case. Electronically, the $GaP_{1-x}As_x$

alloys can thus be considered as bulk layers, without any stress induced by the substrate. From the SRR values and Bragg peak positions, arsenic contents of $GaP_{1-x}As_x$ alloys are then determined accurately. Arsenic compositions x(As) of

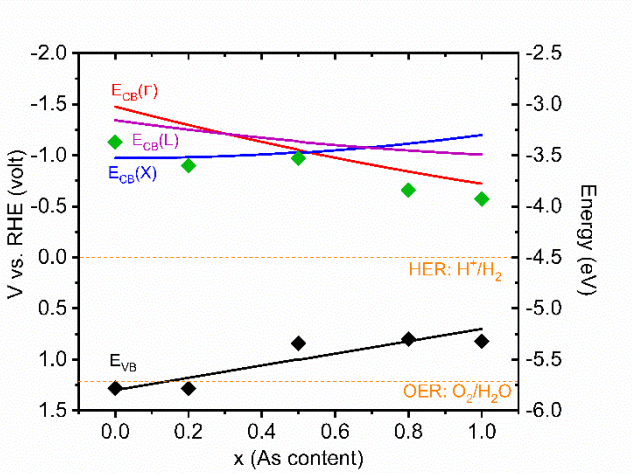

Fig. 4 Experimental flat-band potential (green diamond) as a function of x(As) for $GaP_{1-x}As_x$/Si measured from Mott-Schottky plots. The black diamond dots represent the position of the valence band inferred from the measured flat-band potential and the band gap, as measured by ellipsometry. The theoretical positions of Γ, X and L valleys in the CB and the Γ valley in the VB as a function of x(As) are also shown, considering a linear variation of the VB from x(As)=0 to x(As)=1. [12, 25, 32] The OER potential of 1.23 V is shown as an orange dashed line the CB and the VB as a function of x(As) are also shown, considering a linear variation of the VB from x(As)=0 to x(As)=1. The OER potential of 1.23 V is shown as an orange dashed line.

1.00±0.02, 0.83±0.02, 0.52±0.01, 0.22±0.02 and 0.01±0.01, are obtained respectively and reported in Figure 1a, showing a good consistency with targeted x(As) values, illustrating the very fine control of III-V alloy compositions that can be achieved by MBE.

The sample surface morphology was analyzed by Atomic Force Microscopy (AFM) and Scanning Electron Microscopy (SEM). As shown in **Figure 2**, All $GaP_{1-x}As_x$ alloys present a similar morphology, independently of the As content with a root-mean-square (rms) roughness value in the range of 5–9 nm. By comparison, the wafers show a much lower roughness (~0.8 nm). The large roughness of epitaxial samples is due to the specific growth mode of polar materials ($GaP_{1-x}As_x$) on non-polar substrate (Si),[26] which induces defect generation and a specific morphology.[27,28]

Incident Photon to Current Efficiencies (IPCE) spectra, measured for different samples in a three-electrode PEC cell at the external applied potential of 1 V vs RHE in 0.2 M H_2SO_4 electrolyte (measured pH = 0.35) (see experimental details in Supplementary Data) are reported in **Figure 3a.** A clear red shift of the IPCE low energy edge front is observed as a function of the As composition. The higher the As content within the alloy, the lower the IPCE edge front energy. This trend is strongly correlated to the band gap evolution of $GaP_{1-x}As_x$ alloys as confirmed by the absorption coefficient determination, through spectroscopic ellipsometry measurements (**Figure S4**). IPCE edge fronts at low As contents (x=0 and x=0.22) are less abrupt than those recorded on As-rich photoelectrodes. Additionally, As-poor alloys (0, 0.22 and 0.52) exhibit a maximum IPCE around 30%, whereas As-rich alloys (0.83 and 1) show a maximum IPCE up to 60%. In other words, As-rich alloys absorb more photons and generate more photocurrent. These features are related to the band gap energy reduction and to the indirect-to-direct band gap transition with increasing As content, which is known to occur at x = 0.52 in $GaP_{1-x}As_x$ alloys.[12] **Figure 3b** compares the IPCE spectra for a commercial GaAs wafer (350 µm-thick) and 1 µm-thick GaAs epitaxial layer grown on Si substrate. As mentioned in a recent work,[29] the remarkably high IPCE and the additional low energy contribution observed for the epitaxial III-V/Si sample indicate that despite the large crystal defects density, a fraction of carriers photogenerated in the Si is transferred to the III-V layer, and participates to the total photocurrent. This is not the case for alloys with x > 0.22, in good agreement with the picture given in ref [29], where the carriers transfer is possible from the Si to the III-V layer, only if the valence band lineup is close to zero.

Mott-Schottky (MS) $1/C^2$–E measurements performed in the dark on $GaP_{1-x}As_x$/Si photoanodes with a 0.2 M H_2SO_4 electrolyte (measured pH = 0.35) are given in **Figure S5**. All MS plots show positive slopes indicating n-type doping. Donor densities in the range of 10^{17} and 10^{18} cm^{-3} are measured, which are unexpectedly large values for non-intentionally doped III-V layers grown by MBE. Although contamination (e.g. by carbon atoms) of the Si surface prior to III-V overgrowth cannot be ruled out,[30] the large values measured are more likely explained by the presence of antiphase boundaries in the layers that have been shown to be electrically active, possibly with a donor-like behavior.[31]

Flat-band potentials (V_{fb}) deduced from the A^2/C^2 intercept with the potential x-axis are plotted for the different samples in **Figure 4** (green diamonds). The large values of donor concentrations determined from MS measurements, enable approximation that the Fermi level coincides with the conduction band (CB) level. In this case, V_{fb} corresponds to the CB level versus RHE. By adding the band gap energy determined from spectroscopic ellipsometry measurements, the valence band (VB) positions are deduced (black diamonds). The theoretical positions of the different energy bands of interest for $GaP_{1-x}As_x$, corresponding to the different valleys of the Brillouin zone (Γ, L, X) are superimposed with experimental values in **Figure 4**, following the procedure already used in previous works.[12,25,32] Note that in the semiconductor research community, the CB edge energy is usually referred versus vacuum level (and defined as the electron affinity). In order to compare energy versus RHE and versus vacuum, we consider that the chemical potential for electrons under RHE is shifted by -4.48 eV on the vacuum level.[32] From MS measurements performed on the commercial GaAs wafer, a measured flat-band potential of -0.57 V vs. RHE leads to an electron affinity equal to 3.89 eV, in good agreement with the well-documented 4.07 eV value.[33] The small difference between these two values could be reasonably explained by the presence of surface dipoles and/or surface states. As expected, a weak evolution of the CB energy and a large change of the VB energy as a function

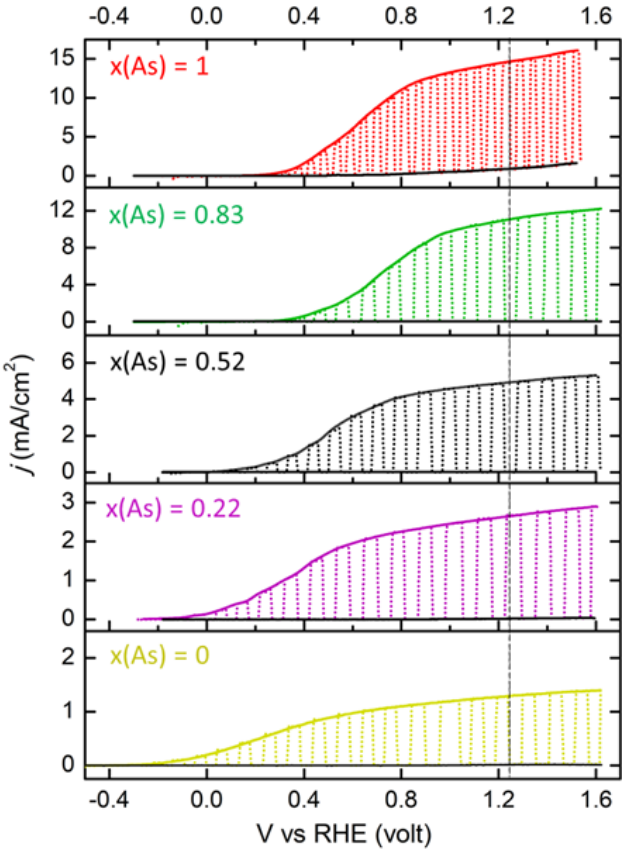

Fig. 5 Chopped-light linear sweep voltammetry curves (scan rate = 50 mV.s^{-1}) for the 1-µm thick epitaxial thin-films of $GaP_{1-x}As_x$ alloys grown on Si with the different compositions x(As) in 0.2M H_2SO_4 (pH = 0.35) electrolyte under simulated sunlight illumination. For each electrode, solid lines show the current recorded under illumination and in the dark.

of the x(As) are observed on the theoretical curves in **Figure 4**, with an indirect (X) to direct (Γ) crossover for x(As)=0.5.[34] The first observation that can be made is the remarkable agreement between the CB and the VB energy variations predicted theoretically and the positions of those deduced from the flat-band potential and ellipsometry measurements. This not only experimentally validates the band bending model used for years in photo-electrochemistry to describe the semiconductor/electrolyte junction, but also implies that, thanks to the fine control of III-V alloys composition provided by epitaxial techniques, it is possible to adjust precisely the position of the VB with respect to the energy levels of the electrolyte. In addition, the O_2/H_2O redox potential was positioned in **Figure 4**, and crosses the valence band maximum for a x(As) composition below 0.2. For an energetically possible OER, the valence band should straddle the O_2/H_2O level. Therefore, in the present study, OER is not expected to occur for photoelectrodes with x(As) contents above 0.2.

The current density vs voltage (*j*-V) measurements were carried out using a three-electrode PEC cell containing a 0.2 M H_2SO_4 electrolyte (measured pH=0.35), in dark and under illumination (100 mW cm^{-2}, AM 1.5G). **Figure 5** shows the *j*-V plots recorded for the different $GaP_{1-x}As_x$/Si photoelectrodes.

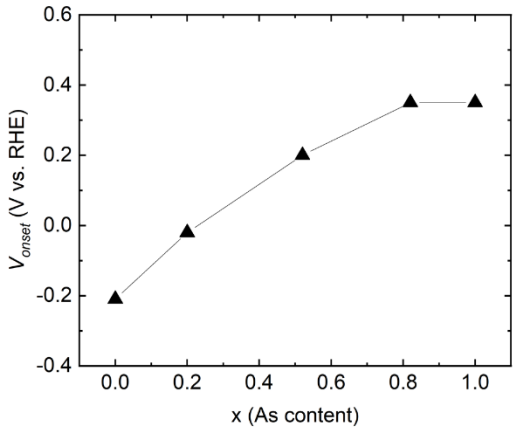

Fig. 6 Variation of the measured onset potentials (V_{onset}) as a function of the As content, x(As), for the $GaP_{1-x}As_x$/Si photoanodes.

Firstly, an increase of the maximum photocurrent density with As composition is observed. Photocurrent densities of 14.62 and 1.34 mA/cm^2 are measured at 1.23 V for GaAs/Si and GaP/Si photoelectrodes, respectively. This photocurrent increase is particularly significant for alloys with an As content higher than 0.52. This is a direct consequence of the alloy band gap decreasing and of indirect to direct band gap transition when the As content increases. These trends are in good agreement with the IPCE data shown in **Figure 3a** and theoretical band structure given in **Figure 4**. Photoelectrodes made from commercial GaAs and GaP substrates present maximum photocurrent densities of 12.22 and 1.27 mA/cm^2, respectively (**Figure S6** in Supplementary Data). In first approximation, similar saturated photocurrents are reached for substrates and epitaxial layers grown on silicon, which confirms the good optical and transport properties of the epilayers grown on the cost-effective Si substrate. Interestingly, the dark current, usually associated with corrosion reactions, remains negligible for all samples, except for the x(As)=1 one. This tends to show that the presence of P at the surface modifies significantly the surface chemistry and possibly mitigates or hampers dark corrosion.

Next, we focus on the onset voltage, (V_{onset}), i.e the potential where a measurable photocurrent (0.1 mA/cm^2) is detected. A Significant V_{onset} increase is observed with increasing As content (**Figure 6**). For ideal semiconductor-electrolyte junctions, the signatures of the band gap reduction and of the valence band OER crossover should in principle be observed in the evolution of the onset potential.[35,36] For the studied III-V/Si PAs, however, the large overpotentials observed at any composition, complicate the onset potential analysis and indicate the strong impact of recombinations on the photocarrier dynamics.[37,38] The deposition of catalysis layers and the development of surface state passivation strategies therefore appear to be mandatory in order to increase the charge transfer rate to the electrolyte and suppress overpotentials. In addition, photocorrosion is also expected to contribute to the physics of the PAs, with threshold potentials that can differ from one alloy to the other. A deeper analysis of the performances of these III-

V/Si photoanodes will thus require the development of efficient protection coatings, which is beyond the scope of this study.

Finally, it is interesting to note that the present work experimentally validates the general concept of band lineup engineering for electrochemical systems. The strategy used here (tuning the semiconductor/electrolyte band alignment through the precise control of alloys composition) may be appealing for many different epitaxial materials used in electrochemistry. Indeed, one can expect that the same approach can be used with all the conventional or nanostructured epitaxial III-V semiconductors (III-N, III-As, III-P and III-Sb), but also with epitaxial oxides or 2D materials commonly used in photo-electrochemistry or in electro-chemistry.

Conclusions

In conclusion, we have studied the photoelectrochemical properties of photoanodes composed of $GaP_{1-x}As_x$ alloys grown on Si substrate with compositions x ranging from 0 to 1. The analysis of IPCE data and photoelectrochemical performance reveals that large photocurrents can be achieved with such photoanodes, comparable to those obtained with photoanodes made of commercial III-V wafers. These results confirm that the epitaxial integration of III-V thin films on Si substrates is of great interest for the development of high efficiency and cost-effective photoelectrodes. We then show that alloying in III-V not only allows to engineer the band gap of photoelectrodes (through sunlight absorption) but also allows to engineer with a fine control the relative positions of the energy bands in the semiconductor and the redox energy levels in the electrolyte. With adapted protecting or passivating layers, this band lineup engineering strategy may allow to address resonantly and selectively specific redox reactions in electrolytes. Thus, it may be of great interest for the design of novel photoelectrochemical devices.

Author Contributions

Mekan Piriyev: XRD, AFM and PEC characterization and data analysis, ellipsometry measurements and data analysis, analysis of light absorption properties. Writing of the original draft. **Gabriel Loget:** PEC measurements and data analysis. **Yoan Léger:** analysis of results and discussion, analysis of the light absorption properties. **Hanh Vi Le:** PEC measurements and data analysis **Lipin Chen:** PEC measurements and data analysis. **Antoine Létoublon:** XRD measurements and data analysis. **Tony Rohel:** design and fabrication the samples. **Christophe Levallois:** ellipsometry measurements and data analysis. **Julie Le Pouliquen:** SEM measurements. **Bruno Fabre:** analysis of PEC results. **Nicolas Bertru:** conception of the idea, design and fabrication of the samples, analysis of results, writing and finalization of the manuscript. **Charles Cornet:** conception of the idea, design and fabrication of the samples, analysis of results, writing and finalization of the manuscript. All authors reviewed and commented on the manuscript.

Conflicts of interest

There are no conflicts to declare.

Acknowledgements

The authors acknowledge RENATECH (French Network of Major Technology Centers) within Nanorennes for technological support, V. Demange and C. Derouet for access to XRD Osirix platform (ScanMAT, UAR 2025 University of Rennes 1-CNRS). This research was supported by the “France 2030” program of the French National Research Agency, NAUTILUS Project (Grant no. ANR-22-PEHY-0013).

Notes and references

1 J.H. Kim, D. Hansora, P. Sharma, J.-W. Jang and J.S. Lee, *Chem. Soc. Rev.*, 2019, **48**, 1908.
2 A. Thakur, D. Ghosh, P. Devi, K.-H. Kim and P. Kumar, *Chem. Eng. J.*, 2020, **397**, 125415.
3 M.G. Walter, E.L. Warren, J.R. McKone, S.W. Boettcher, Q. Mi, E.A. Santori and N.S. Lewis, *Chem. Rev.*, 2010, **110**, 6446.
4 A.I. Osman, N. Mehta, A.M. Elgarahy, M. Hefny, A. Al-Hinai, A.H. Al-Muhtaseb and D.W. Rooney, *Environ. Chem. Lett.*, 2022, **20**, 153.
5 M. Yue, H. Lambert, E. Pahon, R. Roche, S. Jemei and D. Hissel, *Renew. Sust. Energ. Rev.*, 2021, **146**, 111180.
6 J. Tournet, Y. Lee, S.K. Karuturi, H.H. Tan and C. Jagadish, *ACS Energy Lett.*, 2020, **5**, 611.
7 M.R. Shaner, H.A. Atwater, N.S. Lewis and E.W. McFarland, *Energy Environ. Sci.*, 2016, **9**, 2354.
8 Z. Chen, T.F. Jaramillo, T.G. Deutsch, A. Kleiman-Shwarsctein, A.J. Forman, N. Gaillard, R. Garland, K. Takanabe, C. Heske, M. Sunkara, E.W. McFarland, K. Domen, E.L. Miller, J.A. Turner and H.N. Dinh, *J. Mater. Res.*, 2010, **25**, 3.
9 M. Bosi and C. Pelosi, *Prog. Photovolt.: Res. Appl.*, 2007, **15**, 51.
10 S. Saeidi, K.M. Awan, L. Sirbu and K. Dolgaleva, *Appl. Opt.*, 2017, **56**, 5532.
11 C.-Z. Ning, L. Dou and P. Yang, *Nat. Rev. Mater.*, 2017, **2**, 1.
12 I. Vurgaftman, J.R. Meyer and L.R. Ram-Mohan, *J. Appl. Phys.*, 2001, **89**, 5815.
13 S. Hu, M.R. Shaner, J.A. Beardslee, M. Lichterman, B.S. Brunschwig and N.S. Lewis, *Science*, 2014, **344**, 1005.
14 M. Alqahtani, S. Ben-Jabar, M. Ebaid, S. Sathasivam, P. Jurczak, X. Xia, A. Alromaeh, C. Blackman, Y. Qin, B. Zhang, B.S. Ooi, H. Liu, I.P. Parkin and J. Wu, *Opt. Express*, 2019, **27**, A364.
15 Y. Lin, R. Kapadia, J. Yang, M. Zheng, K. Chen, M. Hettick, X. Yin, C. Battaglia, I.D. Sharp, J.W. Ager and A. Javey, *J. Phys. Chem. C.*, 2015, **119**, 2308.
16 D. Kang, J.L. Young, H. Lim, W.E. Klein, H. Chen, Y. Xi, B. Gai, T.G. Deutsch and J. Yoon, *Nat. Energy*, 2017, **2**, 1.

17 C. Jiang, J. Wu, S.J.A. Moniz, D. Guo, M. Tang, Q. Jiang, S. Chen, H. Liu, A. Wang, T. Zhang and J. Tang, *Sustain. Energy Fuels*, 2019, **3**, 814.

18 W.-H. Cheng, M.H. Richter, M.M. May, J. Ohlmann, D. Lackner, F. Dimroth, T. Hannappel, H.A. Atwater and H.-J. Lewerenz, *ACS Energy Lett.*, 2018, **3**, 1795.

19 T. Yao, X. An, H. Han, J.Q. Chen and C. Li, *Adv. Energy Mater.*, 2018, **8**, 1800210.

20 A. Goodrich and M. Woodhouse, *NREL Technical Report*, 2013, NREL/PR-6A20-60126, DOI: 10.2172/1336550.

21 P. Kumar, P. Devi, R. Jain, S.M. Shivaprasad, R.K. Sinha, G. Zhou and R. Nötzel, *Commun. Chem.*, 2019, **2**, 1.

22 M. Alqahtani, S. Sathasivam, L. Chen, P. Jurczak, R. Piron, C. Levallois, A. Létoublon, Y. Léger, S. Boyer-Richard, N. Bertru, J.-M. Jancu, C. Cornet, J. Wu and I.P. Parkin, *Sustain. Energy Fuels*, 2019, **3**, 1720.

23 L. Chen, Y. Léger, G. Loget, M. Piriyev, I. Jadli, S. Tricot, T. Rohel, R. Bernard, A. Beck, J. Le Pouliquen, P. Turban, P. Schieffer, C. Levallois, B. Fabre, L. Pedesseau, J. Even, N. Bertru and C. Cornet, Adv. Sci., 2022, 9, 2101661.

24 I. Lucci, S. Charbonnier, M. Vallet, P. Turban, Y. Léger, T. Rohel, N. Bertru, A. Létoublon, J.-B. Rodriguez, L. Cerutti, E. Tournié, A. Ponchet, G. Patriarche, L. Pedesseau and C. Cornet, *Adv. Funct. Mater.*, 2018, **28**, 1801585.

25 L. Chen, M. Alqahtani, C. Levallois, A. Létoublon, J. Stervinou, R. Piron, S. Boyer-Richard, J.-M. Jancu, T. Rohel, R. Bernard, Y. Léger, N. Bertru, J. Wu, I.P. Parkin and C. Cornet, *Sol. Energy Mater. Sol. Cells*, 2021, **221**, 110888.

26 H. Kroemer, *J. Cryst. Growth*, 1987, **81**, 193.

27 I. Lucci, S. Charbonnier, L. Pedesseau, M. Vallet, L. Cerutti, J.-B. Rodriguez, E. Tournié, R. Bernard, A. Létoublon, N. Bertru, A. Le Corre, S. Rennesson, F. Semond, G. Patriarche, L. Largeau, P. Turban, A. Ponchet and C. Cornet, *Phys. Rev. Mater.*, 2018, **2**, 060401(R).

28 C. Cornet, S. Charbonnier, I. Lucci, L. Chen, A. Létoublon, A. Alvarez, K. Tavernier, T. Rohel, R. Bernard, J.-B. Rodriguez, L. Cerutti, E. Tournié, Y. Léger, M. Bahri, G. Patriarche, L. Largeau, A. Ponchet, P. Turban and N. Bertru, Phys. Rev. Mater., 2020, **4**, 053401.

29 M. Piriyev, G. Loget, Y. Léger, L. Chen, A. Létoublon, T. Rohel, C. Levallois, J. Le Pouliquen, B. Fabre, N. Bertru and C. Cornet, *Sol. Energy Mater. Sol. Cells*, 2023, **251**, 112138.

30 R.N. Sacks and R.A. Pastorello, *Appl. Phys. Lett.*, 1988, **52**, 996.

31 L. Chen, L. Pedesseau, Y. Léger, N. Bertru, J. Even and C. Cornet, Phys. Rev. B, 2022, 106, 165310.

32 C.G. Van de Walle and J. Neugebauer, *Nature*, 2003, **423**, 626.

33 A. Dargys and J. Kundrotas, 1994, *Handbook on physical properties of Ge, Si, GaAs and InP*, Science and Encyclopedia Publishers, Vilnius, Lithuania.

34 C. Robert, M. Perrin, C. Cornet, J. Even and J.M. Jancu, *Appl. Phys. Lett.*, 2012, **100**, 111901.

35 D. Guyomard, *J. Chim. Phys.*, 1986, **83**, 355.

36 B. Iandolo, H. Zhang, B. Wickman, I. Zorić, G. Conibeer and A. Hellman, *RSC Adv.*, 2015, **5**, 61021.

37 R. S. Hutton and L. M. Peter, *J. Electroanal. Chem.*, 1992, **330**, 351.

38 R. Liu, Z. Zheng, J. Spurgeon and X. Yang, *Energy Environ. Sci.*, 2014, **7**, 2504.